How to cite: *Angew. Chem. Int. Ed.* **2023,** *62,* e202302995
doi.org/10.1002/anie.202302995

Photocatalysis

Visible-Light-Reactive Single-Chain Nanoparticles

Kai Mundsinger, Bryan T. Tuten, Lily Wang, Kira Neubauer, Christian Kropf, Megan L. O'Mara,* and Christopher Barner-Kowollik**

Abstract: We introduce a single-chain nanoparticle (SCNP) system capable of catalyzing the photooxidation of nonpolar alkenes up to three times more efficiently than an equivalent small-molecule photosensitizer at an identical concentration. Specifically, we construct a polymer chain constituted of poly(ethylene glycol) methyl ether methacrylate and glycidyl methacrylate which we compact via multifunctional thiol-epoxide ligation and functionalize with Rose Bengal (**RB**) in a one pot reaction, affording SCNPs with a hydrophilic shell and hydrophobic photocatalytic regions. Photooxidation of the internal alkene in oleic acid proceeds under green light. **RB** confined within the SCNP is three times more effective for nonpolar alkenes than free **RB** in solution, which we hypothesize is due to the spatial proximity of the photosensitizing units to the substrate in the hydrophobic region. Our approach demonstrates that SCNP based catalysts can afford enhanced photocatalysis via confinement effects in a homogeneous reaction environment.

Introduction

The last 15 years have seen the emergence of single chain nanoparticles (**SCNP**) as a powerful macromolecular architecture generated by the folding of individual synthetic polymer chains via specific crosslinking mechanisms into compacted entities.[1] A plethora of compaction approaches has been explored, ranging from reversible concepts based on hydrogen bonding[2] and photochemical processes[3] to irreversible covalent compaction via thermally driven processes.[4] The field has been reviewed extensively by several research teams,[5] including us,[6] highlighting the current state-of-the-art and more critically the open application frontiers for these materials including in sensors, delivery agents, and—most prominently—catalysis.[7]

We and others have explored transition metal-driven catalysis exploiting SCNPs as a recoverable catalytic system, fusing the advantages of heterogeneous catalysis (simple recovery of the catalyst) with the efficacy of homogeneous catalytic systems.[8] For example, we have incorporated Pt-complexes into SCNPs, dually using the Pt-complex, i.e. for compaction of the chains and as catalytic moieties to catalyze hydroamination reactions.[9] Additionally, some photoactivated catalytic SCNPs have been explored previously by Palmans and co-workers in singlet oxygen producing SCNPs[10] as well as the Elacqua team who utilized folding styrylpyrene moieties via visible light with pendant photoredox-active triarylpyrylium tetrafluoroborate groups.[11] While there is clear evidence that SCNP-driven catalysis is at least as effective as comparative concentrations of free transition metals in solution and despite the added benefit of catalyst recyclability, little attention has been paid to constructing SCNP environments that will enhance catalysis over the free solution-based process. SCNPs should in principle constitute ideal nano-catalysts with increased catalytic activity, as are their natural analogues, i.e. proteins and enzymes.[12] Two approaches are

[*] Dr. K. Mundsinger, Dr. B. T. Tuten, Prof. C. Barner-Kowollik
School of Chemistry and Physics,
Queensland University of Technology (QUT)
4000 Brisbane QLD (Australia)
and
Centre for Materials Science,
Queensland University of Technology (QUT)
4000 Brisbane QLD (Australia)
E-mail: bryan.tuten@qut.edu.au
christopher.barnerkowollik@qut.edu.au
L. Wang, Prof. M. L. O'Mara
Research School of Chemistry,
College of Science,
The Australian National University
2601 Canberra, Australian Capital Territory (Australia)
E-mail: megan.omara@anu.edu.au
Dr. K. Neubauer, Dr. C. Kropf
Henkel AG & Co. KGaA
Henkelstraße 67, 40589 Düsseldorf (Germany)
Prof. M. L. O'Mara
Australian Institute for Bioengineering and Nanotechnology,
The University of Queensland
4072 St Lucia, QLD (Australia)
Prof. C. Barner-Kowollik
Institute of Nanotechnology (INT),
Karlsruhe Institute of Technology (KIT)
Hermann-von-Helmholtz-Platz 1, 76344 Eggenstein-Leopoldshafen (Germany)

feasible to increase catalytic activity within an SCNP via tuning of the reaction environment.

In analogy to recent developments in heterogeneous catalysis, placing the catalyst within a confined environment opens the possibility of synergistic effects arising from the combination of catalyst and its environment.[13] Ideally, consideration is given to designing a complementary environment or catalytic region within the SCNP, tailored to a specific substrate.[14] While certainly the most rational approach, it requires a deep theoretical understanding of the ideal catalytic environment and—perhaps even more challenging—the subsequent construction of such an environment during the SCNP synthesis. Within reasonable chemical effort, such environments are currently unobtainable without possibly resorting to sequence-defined polymers with bespoke folding points leading to their selective point folding to create the optimum chemical environment for the catalytic site. An alternative approach that inspired the current study rests on our previous observation that photoreactive units employed to compact single-chain nanoparticles, here specifically visible light-reactive styrylpyrene entities, feature a strongly increased quantum yield for their [2+2] dimerization due to their confinement compared to the free solution.[15] We have furthermore incorporated sophisticated computational work to guide our synthetic strategy to devise a more advanced SCNP design. We opted to investigate oxidations, as these lend themselves to be triggered photochemically. Excitation of triplet oxygen ($^3O_2$) to its singlet state ($^1O_2$) via energy transfer from a photosensitizer[16] facilitates oxidation of olefins[17] under ambient conditions. Careful selection of the photosensitizer allows for the generation of $^1O_2$ at a chosen color of light, from ultraviolet[18] to visible[19] into the infrared.[20]

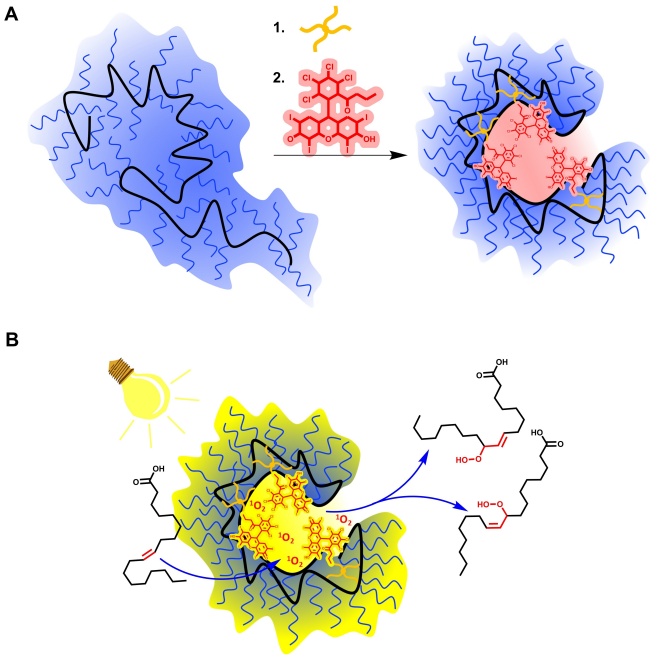

Scheme 1. **A)** Crosslinking (orange), and Rose Bengal functionalization, of a poly(ethylene glycol) methacrylate based polymer into a single-chain nanoparticle generates a discrete hydrophobic region (red) within a hydrophilic exterior (blue). **B)** Hydrophobic molecules (oleic acid) are driven into the hydrophobic region, oxidized under irradiation via generation of singlet oxygen and the products are subsequently expelled.

Results and Discussion

Herein, we translate our earlier observed photochemical reaction enhancement enabled by confined environments to the realm of photocatalysis. We use insights gained from molecular dynamics simulation to guide the design strategy of our SCNPs. We design a catalytically active SCNP that exhibits a core–shell like morphology with a hydrophilic exterior contrasting the hydrophobic interior serving as catalytic region as depicted in Scheme 1.[21] Specifically, we fold single polymer chains into SCNPs via thiol-epoxy ring opening utilizing multifunctional thiols and embed photoactive Rose Bengal (**RB**) units into the polymer via thiol-ene click reactions. We subsequently assess the photocatalytic SCNP against an identical concentration of free **RB** in free solution demonstrating significantly increased photooxidative activity. To examine the formation and distribution of hydrophobic regions in an SCNP constituted by our monomers of choice, polymer templates were benchmarked using molecular dynamics (**MD**) simulations of block, statistical, and periodic ($A(AAAAB)_{52}A$) copolymers (refer to Figure S3). **MD** simulations offer the benefit of testing various polymer architectures and compositions simultaneously and rapidly, while also providing detailed insight into the resulting polymer properties that purely experimental methods do not allow, for instance distribution of polar and nonpolar groups within the polymer. We aimed for molar masses between 50 kg mol^{-1} and 100 kg mol^{-1} to provide a sufficiently large environment for the bulky photoactive moieties with 20 mol % crosslinkable units as earlier studies demonstrated molar masses above 20 kg mol^{-1} and 5–30 mol % folding units to be ideal for SCNP compaction.[22] In each case, a 262 unit polymer was constructed using a 4/1 molar ratio of poly(ethylene glycol) methyl ether methacrylate (**MPEGMA**) and glycidyl methacrylate (**GMA**). Prior to 500 ns of non-restrained **MD** simulation, the extended polymer was allowed to compact in the simulation. All polymers condensed and formed a hydrophilic surface with transient hydrophobic pockets. In the block copolymer, the hydrophobic **GMA** units clustered into a single channel along the polymer surface (Figure S3a). In the statistical and periodic copolymers, smaller hydrophobic regions were interspersed throughout the compacted structure (Figure S3b–c). This difference was reflected in the solvent accessible surface area (SASA) (Figure S5) of the polymers; the block copolymer had a slightly higher solvent accessible surface area (SASA = 173.3 ± 3.0 nm^2) than the statistical (SASA = 171.9 ± 3.0 nm^2) and periodic (SASA = 171.6 ± 3.3 nm^2) copolymers. The mean radius of gyration however was 2.24 nm for all three polymers (σ = 0.01 nm, Figure S5). Guided by these findings, we opted to synthesize a statistical copolymer instead of a block-copolymer, placing the hydro-

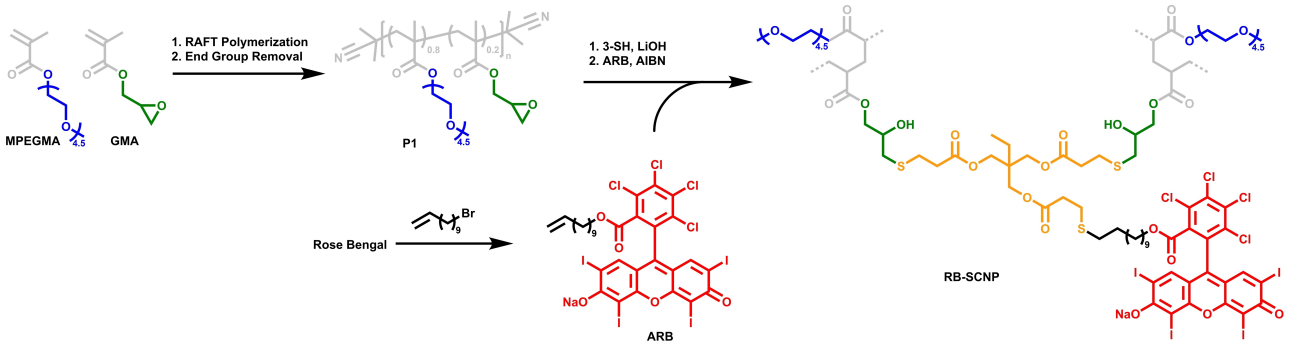

Scheme 2. Synthesis route to Rose Bengal functionalized single-chain nanoparticles (**RB-SCNP**). Reversible addition-fragmentation chain-transfer (RAFT) polymerization of poly(ethylene glycol) methyl ether methacrylate (**MPEGMA**) and glycidyl methacrylate (**GMA**) and subsequent end group removal with azobisisobutyronitrile (**AIBN**). Intramolecular crosslinking of the linear polymer (**P1**) with trimethylolpropane tris(3-mercaptopropionate) (**3-SH**) via ring-opening of epoxides by thiols and concurrent functionalization with alkene functionalized Rose Bengal (**ARB**) via thiol-ene click reaction.

phobic areas throughout the particle without sacrificing solvent accessible surface area, enabling substrates to come into contact with the active moieties.

The synthesis route is outlined in Scheme 2. 11-Bromo undecane was coupled to **RB** via halide substitution to afford alkene functionalized **RB** (**ARB**). **MPEGMA** was copolymerized (4/1 molar ratio) with **GMA** via reversible addition-fragmentation chain-transfer (RAFT) polymerization using azobisisobutyronitrile as initiator and 2-cyano-2-propyl benzodithioate as chain transfer agent to yield the linear polymer **P1**. Subsequently, **P1** was intramolecularly crosslinked with trimethylolpropane tris(3-mercaptopropionate) (**3-SH**) and functionalized with **ARB** at the crosslinking sites to afford **RB-SCNP**.

For the detailed synthetic procedures, refer to the Supporting Information Section 4. Successful functionalization of **RB-SCNP** with **RB** was indicated by the polymer's UV response increasing orders of magnitude compared to the parent polymer **P1** (Figure 1 top and bottom right).

Polymer solutions subjected to preparative size exclusion chromatography (SEC) retained their UV absorbance ($\lambda_{max} = 565$ nm), which was used to calibrate the concentration of photoactive units in all subsequent experiments. Upon crosslinking, despite simultaneous mass gain due to functionalization with **RB**, the apparent molar mass of **P1** decreased by 16 % from 69.1 kg mol^{-1} to 58.3 kg mol^{-1} for **RB-SCNP** (Figure 1 top right to bottom right) and the hydrodynamic radius (r_H) observed in SEC decreased 8 % (Figure 1 top left). Dynamic light scattering (DLS) was used to confirm polymer folding and showed a 36 % decrease of r_H respectively (Figure 1 bottom left), further evidencing compaction of the linear polymers into single-chain nanoparticles.[23]

The photooxidative properties of **RB-SCNP** were investigated by irradiating solutions of oleic acid, *trans*-3-hexenoic acid and *cis*-butene-1,4-diol in mixtures of acetonitrile-d_3 and water (10 vol.–%) in the presence of **P1**, free **RB**, **P1** and free **RB**, and **RB-SCNP** (concentration of photoactive compound 4.3 µg mL^{-1}, 3.7 nM, in all experiments, for details refer to Supporting Information section 3.1). Substrates were used in a sufficiently large excess to ensure exhaustion of the catalyst, enabling calculation of turnover numbers (TON). Each experiment was performed in triplicate, the results are summarized in Table 1. The conversion to the oxidized product was determined via integration and comparison of the aforementioned ^{1}H NMR spectroscopic resonances (Figure 2, for details refer to the Supporting Information section 3.6). Irradiation of, for example, oleic acid in the presence of **RB** resulted in a decrease of the integrated resonance intensity at 5.3 ppm, corresponding to the protons at the double bond and appearance of two new resonances at 5.6 ppm and 4.1 ppm indicating conversion of the double bond into a hydroperoxide species thereby shifting the double bond along the carbon chain.[24] Irradiation of the substrate alone had no influence on its integrity as confirmed via ^{1}H NMR spectroscopy (Figure S9). Substrate irradiated in the presence of **P1**, also showed no observable change of the substrate (Figure S10). Importantly, we observed a threefold increase when, instead of free **RB**, we added **RB-SCNP** with an

Table 1: Conversion and turnover number (TON) obtained in the irradiation experiments described above.

Active Compound	Substrate[a]	µmol mL^{-1}	Conversion %[b]	Conversion mmol	TON[c]
None	OA	24	0	0	0
P1	OA	24	0	0	0
P1 and **RB**	OA	24	11.6	5	700
RB	OA	24	12.7	6	800
RB-SCNP	OA	24	42.9	20	2800
RB	OA	143	7.0	20	2700
RB-SCNP	OA	143	25.3	72	9800
RB	HA	143	2.0	6	800
RB-SCNP	HA	143	1.5	4	600
RB	BD	547	1.1	12	1600
RB-SCNP	BD	547	1.5	16	2200

[a] OA: oleic acid, HA: *trans*-3-hexenoic acid, BD: *cis*-butene-1,4-diol. [b] ^{1}H NMR spectroscopy, average of resonances 1, 2 and 3 (refer to Figure 2), [c] molar ratio of photoactive compound and reaction product.

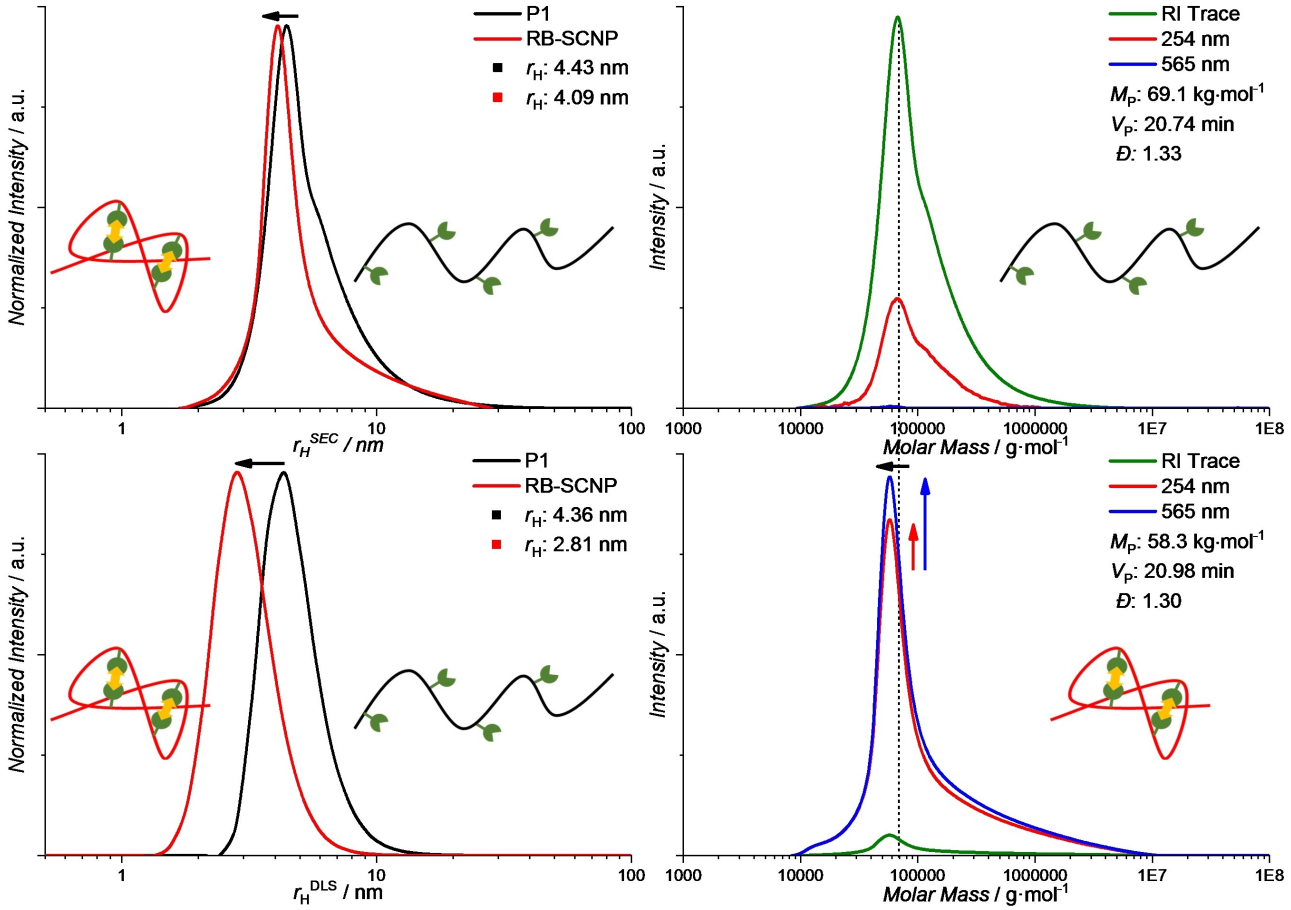

Figure 1. Top left: Size distributions of linear **P1** (black) and Rose Bengal functionalized single-chain nanoparticles (**RB-SCNP**) (red) via size exclusion chromatography (SEC) calibrated for hydrodynamic radii. Bottom left: Size distributions of **P1** (black) and **RB-SCNP** (red) as hydrodynamic radii via dynamic light scattering. Top right: SEC traces of **P1** showing the relative intensities of differential refractive index (green) versus UV detection (254 nm in red and 565 nm in blue). Bottom right: SEC traces of **RB-SCNP** showing the relative intensities of differential refractive index (green) versus UV detection (254 nm in red and 565 nm in blue). *Mp* of **P1** illustrated as dashed line in black.

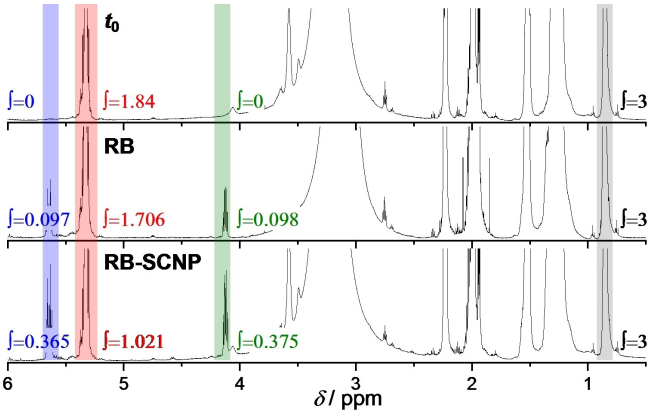

Figure 2. ^{1}H NMR spectrum before (t_0) and after irradiation (λ_{max} = 565 nm) of oleic acid (24 μmol mL^{-1}) in the presence of free Rose Bengal (**RB**) and Rose Bengal functionalized single-chain nanoparticles (**RB-SCNP**) (4 nmol mL^{-1} photoactive moiety) in acetonitrile-d_3 and water (10 vol.-%). Resonances used for quantification highlighted in blue (1), red (2), green (3) and reference in grey (4).

identical concentration of photoactive units. Free **RB** achieved a turnover number—derived from the molar ratio of photoactive units and converted oleic acid—of 800 while **RB-SCNP** achieved 2800, which is a remarkable increase in catalytic activity. Addition of **P1** to free **RB** resulted in a TON of 700, which is - within the error margin - the same conversion as free **RB**, evidencing that placement of the photosensitizer in the hydrophobic region of the SCNP, via a chemical bond, is key.

The influence of polarity is further evidenced by the results of the *trans*-3-hexenoic acid oxidation. A shorter and more polar fatty acid in comparison to oleic acid, however not fully water soluble, exhibited not only lower conversion and turnover in general but interestingly free **RB** achieved a slightly greater TON of 800 versus **RB-SCNP** only resulting in a TON of 600. Oxidation of cis-butene-1,4-diol, a completely water miscible but less polar substrate, resulted in similar TONs compared to oleic acid oxidized with free **RB**, 1600 with free **RB** and 2200 using **RB-SCNP**, demonstrating only a minor effect of the SCNP.

These results are supported by our **MD** simulations (Supporting Information section 2.2). A computational mod-

el of **RB-SCNP** was generated with 7 intramolecular crosslinks, with **ARB** attached to 5 of those crosslinking sites (Figure S4). Briefly, the polymer was allowed to condense, then the crosslinking sites were chosen based on the physical distance of crosslinkable groups (epoxides) to replicate the experimental process of adding crosslinker to the polymer in solution. Despite using a trifunctional crosslinker we decided to only simulate "bimolecular" crosslinks as previous studies found that multivalent crosslinking is a rare occurrence even when using polyfunctional crosslinking chemistries.[25] Five molecules of oleic acid were added to the solution surrounding **RB-SCNP**. Two sets of simulations were performed in triplicate each, an initial screening set in water; and a second set in a solution of acetonitrile with 10 vol.-% water to match experimental conditions. Throughout the simulations, **RB** moieties were observed in individual, transient hydrophobic microenvironments (pockets) that were accessible to solvent and substrate. Representative visualizations of **RB** on the hydrophilic surface and within a hydrophobic pocket are illustrated in Figure 3. Oleic acid associated with the polymer and remained within the hydrophobic region throughout the trajectory, forming dynamic contacts with **RB** for 5% of the trajectory (Figure 3) indicating that nonpolar molecules are driven into the active regions of the particle. In acetonitrile and water (10 vol.-%) association of oleic acid with **RB** was also observed, albeit to a smaller extent (3% of the trajectory near the polymer). The association of oleic acid with the hydrophobic region places it in direct proximity to the generated singlet oxygen, facilitating oxidation. In contrast, small molecule photosensitizers in solution relies solely on the statistical probability of oleic acid encountering dissolved singlet oxygen.

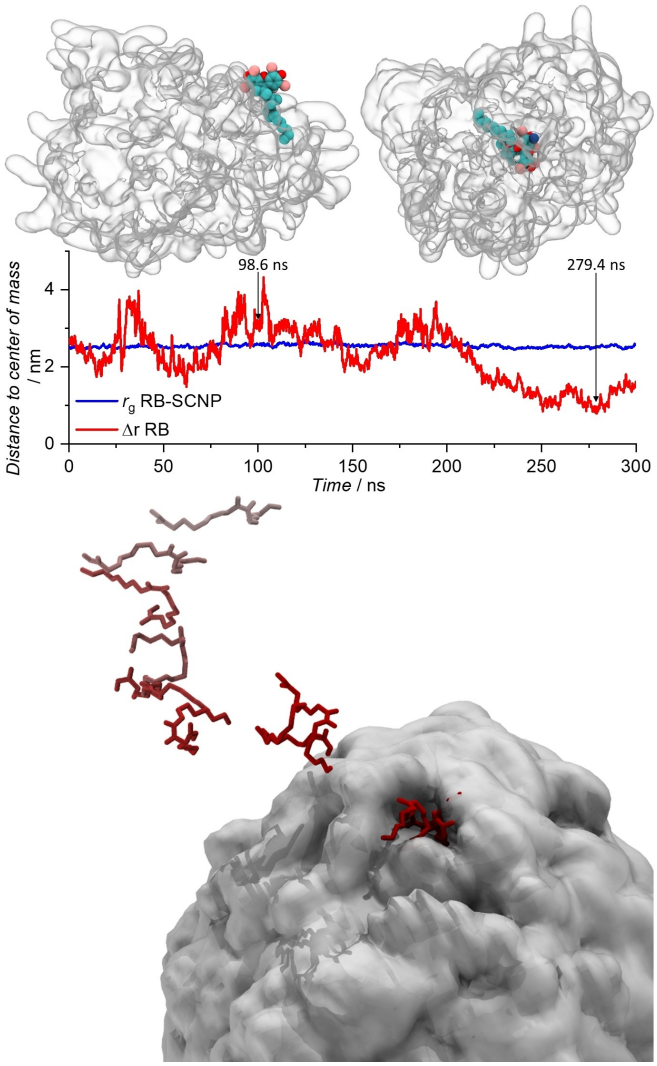

Figure 3. Top: Snapshots of the position of one Rose Bengal (**RB**) moiety within the Rose Bengal functionalized single-chain nanoparticle (**RB-SCNP**) at two frames (98.6 ns and 279.4 ns) during the simulation in acetonitrile with 10% water. Mid: Distance of the depicted **RB** moiety from the center of mass and r_g over time. Bottom: Trajectory of oleic acid approaching **RB-SCNP** in water. Shown as snapshots in 0.2 ns intervals. Proximity of oleic acid to **RB** illustrated as grey to red gradient, contact with **RB** occurring 5% of the time.

Conclusion

Hydrophilic surface—hydrophobic pocket SCNP design was guided by **MD** simulations to optimize the distribution of polarity and solvent accessible surface within single chain nanoparticles (SCNPs). Placement of a photosensitizing moiety within the confined environment of the designed nano-reactor was investigated regarding its photocatalytic activity under visible light irradiation. The combination of the tailored polarity and confinement within the particle resulted in a three-fold increase of turnover compared to the small molecule photosensitizer in solution. The herein introduced visible light reactive SCNPs highlight their potential in homogeneous catalysis driven by synergistic effects between confinement of the catalytic site and its chemical surrounding. Inclusion of further functionality into the SCNP system, for example transition metal complexes, could be used to establish a 'catalytic diad' and progress from oxidation to cleavage of the substrate.

Acknowledgements

C. B.-K., B. T. T. and M. O. are grateful to Henkel AG & Co. KGaA for funding the current research project. C.B.-K. is additionally grateful for an Australian Research Council (ARC) Laureate Fellowship enabling his photochemical research program as well as continued key support from the Queensland University of Technology (QUT). The Central Analytical Research Facility (CARF) at QUT is gratefully acknowledged for access to analytical instrumentation, supported by QUT's research portfolio. Access to computational resources from the National Computational Infrastructure (NCI) and the Pawsey Supercomputing Centre are gratefully acknowledged under the National Computational Merit Allocation Scheme. Open Access publishing facilitated by Queensland University of Technology, as part of the Wiley - Queensland University of Technology agreement via the Council of Australian University Librarians.

Conflict of Interest

The authors have submitted a priority patent application based on the technology described in the manuscript.

Data Availability Statement

The data that support the findings of this study are available in the Supporting Information of this article. Data of the molecular dynamics simulations can be found under the following repository: https://github.com/OMaraLab/single_chain_nanoparticles_materials.

Keywords: Molecular Dynamics · Polymers · Reaction Confinement · Single-Chain Nanoparticle · Singlet Oxygen

[1] J. Rubio-Cervilla, E. González, J. A. Pomposo, *Nanomaterials* **2017**, *7*, 341.
[2] O. Altintas, P. Gerstel, N. Dingenouts, C. Barner-Kowollik, *Chem. Commun.* **2010**, *46*, 6291–6293.
[3] O. Altintas, J. Willenbacher, K. N. R. Wuest, K. K. Oehlenschlaeger, P. Krolla-Sidenstein, H. Gliemann, C. Barner-Kowollik, *Macromolecules* **2013**, *46*, 8092–8101.
[4] a) J. B. Beck, K. L. Killops, T. Kang, K. Sivanandan, A. Bayles, M. E. Mackay, K. L. Wooley, C. J. Hawker, *Macromolecules* **2009**, *42*, 5629–5635; b) C. T. Adkins, J. N. Dobish, S. Brown, E. Harth, *ACS Macro Lett.* **2013**, *2*, 710–714; c) C. T. Adkins, H. Muchalski, E. Harth, *Macromolecules* **2009**, *42*, 5786–5792; d) I. Perez-Baena, I. Asenjo-Sanz, A. Arbe, A. J. Moreno, F. Lo Verso, J. Colmenero, J. A. Pomposo, *Macromolecules* **2014**, *47*, 8270–8280; e) D. Chao, X. Jia, B. Tuten, C. Wang, E. B. Berda, *Chem. Commun.* **2013**, *49*, 4178–4180.
[5] a) R. Chen, E. B. Berda, *ACS Macro Lett.* **2020**, *9*, 1836–1843; b) A. M. Hanlon, C. K. Lyon, E. B. Berda, *Macromolecules* **2016**, *49*, 2–14; c) E. Verde-Sesto, A. Arbe, A. J. Moreno, D. Cangialosi, A. Alegría, J. Colmenero, J. A. Pomposo, *Mat. Horiz.* **2020**, *7*, 2292–2313; d) J. Rubio-Cervilla, E. González, J. A. Pomposo, in *Single-Chain Polymer Nanoparticles*, Wiley-VCH, Weinheim, **2017**, pp. 341–388.
[6] a) O. Altintas, T. S. Fischer, C. Barner-Kowollik, in *Single-Chain Polymer Nanoparticles*, Wiley-VCH, Weinheim, **2017**, pp. 1–45; b) H. Frisch, B. T. Tuten, C. Barner-Kowollik, *Isr. J. Chem.* **2020**, *60*, 86–99.
[7] J. Chen, K. Li, J. S. L. Shon, S. C. Zimmerman, *J. Am. Chem. Soc.* **2020**, *142*, 4565–4569.
[8] H. Rothfuss, N. D. Knöfel, P. W. Roesky, C. Barner-Kowollik, *J. Am. Chem. Soc.* **2018**, *140*, 5875–5881.
[9] N. D. Knöfel, H. Rothfuss, J. Willenbacher, C. Barner-Kowollik, P. W. Roesky, *Angew. Chem. Int. Ed.* **2017**, *56*, 4950–4954.
[10] Y. Liu, S. Pujals, P. J. M. Stals, T. Paulöhrl, S. I. Presolski, E. W. Meijer, L. Albertazzi, A. R. A. Palmans, *J. Am. Chem. Soc.* **2018**, *140*, 3423–3433.
[11] J. J. Piane, S. Huss, L. T. Alameda, S. J. Koehler, L. E. Chamberlain, M. J. Schubach, A. C. Hoover, E. Elacqua, *J. Polym. Sci.* **2021**, *59*, 2867–2877.
[12] H. Bisswanger, in *Enzyme: Struktur, Kinetik und Anwendungen*, 1st ed. Wiley-VCH, Weinheim, **2015**.
[13] a) F. Ziegler, J. Teske, I. Elser, M. Dyballa, W. Frey, H. Kraus, N. Hansen, J. Rybka, U. Tallarek, M. R. Buchmeiser, *J. Am. Chem. Soc.* **2019**, *141*, 19014–19022; b) S.-M. Wu, X.-Y. Yang, C. Janiak, *Angew. Chem. Int. Ed.* **2019**, *58*, 12340–12354.
[14] a) V. Mouarrawis, R. Plessius, J. I. van der Vlugt, J. N. H. Reek, *Front. Chem.* **2018**, *6*, 623; b) S. Pullen, G. H. Clever, in *Reactivity in Confined Spaces, Vol. 1* (Eds.: G. Lloyd, R. S. Forgan), Royal Society of Chemistry, **2021**, pp. 247–281.
[15] H. Frisch, J. P. Menzel, F. R. Bloesser, D. E. Marschner, K. Mundsinger, C. Barner-Kowollik, *J. Am. Chem. Soc.* **2018**, *140*, 9551–9557.
[16] C. S. Foote, *Photochem. Photobiol.* **1991**, *54*, 659–659.
[17] A. A. Frimer, *Chem. Rev.* **1979**, *79*, 359–387.
[18] M. P. Merville, J. Decuyper, M. Lopez, J. Piette, A. Van De Vorst, *Photochem. Photobiol.* **1984**, *40*, 221–226.
[19] a) H. Stiel, K. Teuchner, A. Paul, D. Leupold, I. E. Kochevar, *J. Photochem. Photobiol. B* **1996**, *33*, 245–254; b) A. Borodziuk, P. Kowalik, M. Duda, T. Wojciechowski, R. Minikayev, D. Kalinowska, M. Klepka, K. Sobczak, Ł. Kłopotowski, B. Sikora, *Nanotechnology* **2020**, *31*, 465101; c) A. Alqerban, *Pharmaceuticals* **2021**, *14*, 48.
[20] a) L. Hong, J.-L. Wang, J.-X. Geng, Y.-H. Zhao, G.-X. Zhou, J. Zhang, L.-W. Liu, J.-L. Qu, *Colloids Surf. B* **2021**, *198*, 111500; b) M. G. C. Machado, M. A. de Oliveira, E. G. Lanna, R. P. Siqueira, G. Pound-Lana, R. T. Branquinho, V. C. F. Mosqueira, *Biomed. Pharmacother.* **2022**, *145*, 112464.
[21] J. F. Hoffmann, A. H. Roos, F.-J. Schmitt, D. Hinderberger, W. H. Binder, *Angew. Chem. Int. Ed.* **2021**, *60*, 7820.
[22] J. Engelke, B. T. Tuten, R. Schweins, H. Komber, L. Barner, L. Plüschke, C. Barner-Kowollik, A. Lederer, *Polym. Chem.* **2020**, *11*, 6559–6578.
[23] E. Blasco, B. T. Tuten, H. Frisch, A. Lederer, C. Barner-Kowollik, *Polym. Chem.* **2017**, *8*, 5845–5851.
[24] a) M. N. Alberti, M. Orfanopoulos, *Eur. J. Chem.* **2010**, *16*, 9414–9421; b) D. A. Singleton, C. Hang, M. J. Szymanski, M. P. Meyer, A. G. Leach, K. T. Kuwata, J. S. Chen, A. Greer, C. S. Foote, K. N. Houk, *J. Am. Chem. Soc.* **2003**, *125*, 1319–1328.
[25] J. Steinkoenig, H. Rothfuss, A. Lauer, B. T. Tuten, C. Barner-Kowollik, *J. Am. Chem. Soc.* **2017**, *139*, 51–54.

Manuscript received: February 28, 2023
Accepted manuscript online: March 7, 2023
Version of record online: April 26, 2023